Bottomonium dissociation in a rotating plasma

Nelson R. F. Braga[*] and Yan F. Ferreira[†]

Instituto de Física, Universidade Federal do Rio de Janeiro, Rio de Janeiro 21941-909, Brazil

(Received 23 September 2023; accepted 13 October 2023; published 13 November 2023)

Heavy vector mesons provide important information about the quark gluon plasma (QGP) formed in heavy ion collisions. This happens because the fraction of quarkonium states that are produced depends on the properties of the medium. The intensity of the dissociation process in a plasma is affected by the temperature, the chemical potential and the presence of magnetic fields. These effects have been studied by many authors in the recent years. Another important factor that can affect the dissociation of heavy mesons, and still lacks of a better understanding, is the rotation of the plasma. Noncentral collisions form a plasma with angular momentum. Here we use a holographic model to investigate the thermal spectrum of bottomonium quasistates in a rotating medium in order to describe how a nonvanishing angular velocity affects the dissociation process.

DOI: 10.1103/PhysRevD.108.094017

I. INTRODUCTION

Heavy ion collisions, produced in particle accelerators, lead to the formation of a new state of matter, a plasma where quarks and gluons are deconfined. This so-called QGP behaves like a perfect fluid and lives for a very short time [1–4]. The study of this peculiar state of matter is based on the analysis of the particles that are observed after the hadronization process occur and the plasma disappears. For this to be possible, it is necessary to understand how the properties of the QGP, like temperature (T) and density (μ), affect the spectra that reach the detectors. In particular, quarkonium states, like bottomonium, are very interesting since they survive the deconfinement process that occur when the QGP is formed. They undergo a partial dissociation, with an intensity that depends on the characteristics of the medium, like T and μ. So, it is important to find it out how the properties of the plasma affect the dissociation.

Bottomonium quasistates in a thermal medium can be described using holographic models [5–11] see also [12–14]. In particular, the improved holographic model proposed in [8], which will be considered here, involves three energy parameters; one representing the heavy quark mass, another associated with the intensity of the strong interaction (string tension) and another with the nonhadronic decay of quarkonium. This model provides good estimates for masses and decay constants.

Besides temperature, density and magnetic fields, another, less studied, property that affects the thermal behavior is the rotation of the QGP, that occurs in noncentral collisions. For previous works about the rotation effects in the QGP, see for example [15–32]. In particular, a holographic description of the QGP in rotation can be found in Refs. [22,28]. A rotating plasma with uniform rotational speed is described holographically in these works by a rotating black hole with cylindrical symmetry. Rotation is obtained by a coordinate transformation and the holographic model obtained predicts that plasma rotation decreases the critical temperature of confinement/deconfinement transition [28]. For a very recent study of charmonium in a rotating plasma see [33].

The purpose of this work is to study how rotation of the plasma affects the thermal spectrum of bottomonium quasistates. In other words, we want to understand what is the effect of rotation in the dissociation process of $b\bar{b}$. We will follow two complementary approaches. One is to calculate the thermal spectral functions and the other is to find the quasinormal models associated with bottomonium in rotation.

The organization is the following. In Sec. II we present a holographic model for bottomonium in a rotating plasma. In Sec. III we work out the equations of motion for the fields that describe the quasistates. In Sec. IV we discuss the solutions, taking into account the incoming wave boundary conditions on the black hole horizon. In Sec. V we calculate the spectral functions for bottomonium and in Sec. VI we present the complex frequencies of the quasinormal modes. Finally, Sec. VII contains our conclusions and discussions about the results obtained.

[*]braga@if.ufrj.br
[†]yancarloff@pos.if.ufrj.br

TABLE I. Comparison of bottomonium masses and decay constants obtained experimentally [34] and from the tangent model.

Bottomonium masses and decay constants				
State	Experimental masses (MeV)	Masses on the tangent model (MeV)	Experimental decay constants (MeV)	Decay constants on the tangent model (MeV)
1S	9460.30 ± 0.26	6905	715.0 ± 4.8	719
2S	10023.26 ± 0.31	8871	497.4 ± 4.5	521
3S	10355.2 ± 0.5	10442	430.1 ± 3.9	427
4S	10579.4 ± 1.2	11772	341 ± 18	375

II. HOLOGRAPHIC MODEL FOR QUARKONIUM IN THE PLASMA

Vector mesons are represented holographically by a vector field $V_m = (V_t, V_1, V_2, V_3, V_z)$, that lives, in the case of a nonrotating plasma, in a five-dimensional anti–de Sitter (AdS$_5$) black hole space with metric

$$\mathrm{d}s^2 = \frac{R^2}{z^2}\left(-f(z)\mathrm{d}t^2 + (\mathrm{d}x^1)^2 + (\mathrm{d}x^2)^2 + (\mathrm{d}x^3)^2 + \frac{1}{f(z)}\mathrm{d}z^2\right), \tag{1}$$

with

$$f(z) = 1 - \frac{z^4}{z_h^4}. \tag{2}$$

The constant R is the AdS radius and the Hawking temperature of the black hole, given by

$$T = \frac{1}{\pi z_h}, \tag{3}$$

is identified with the temperature of the plasma.

The action integral for the field has the form

$$I = \int \mathrm{d}^4x \int_0^{z_h} \mathrm{d}z \sqrt{-g}\mathcal{L}, \tag{4}$$

with the Lagrangian density

$$\mathcal{L} = -\frac{1}{4g_5^2}\mathrm{e}^{-\phi(z)} g^{mp} g^{nq} F_{mn} F_{pq}, \tag{5}$$

where $F_{mn} = \nabla_m V_n - \nabla_n V_m = \partial_m V_n - \partial_n V_m$, with ∇_m being the covariant derivative. The dilatonlike background field $\phi(z)$ is [7,8]

$$\phi(z) = \kappa^2 z^2 + Mz + \tanh\left(\frac{1}{Mz} - \frac{\kappa}{\sqrt{\Gamma}}\right). \tag{6}$$

The backreaction of $\phi(z)$ on the metric is not taken into account. This modified dilaton is introduced in order to obtain an approximation for the values of masses and decay constants of heavy vector mesons. The three parameters of the model are fixed at zero temperature to give the best values for these quantities, specially the decay constants, compared with the experimental values for bottomonium found in the particle data group table [34]; $\kappa_b = 2.45$ GeV, $\sqrt{\Gamma_b} = 1.55$ GeV and $M_b = 6.2$ GeV. The results are presented in Table I.

In order to have some characterization of the quality of the fit, one can define the root mean square percentage error (RMSPE) as

$$\mathrm{RMSPE} = 100\% \times \sqrt{\frac{1}{N - N_p}\sum_{i=1}^{N}\left(\frac{y_i - \hat{y}_i}{\hat{y}_i}\right)^2}, \tag{7}$$

where $N = 8$ is the number of experimental points (4 masses and 4 decay constants), $N_p = 3$ is the number of parameters of the model, the y_i's are the values of masses and decay constants predicted by the model and the $\hat{y}_i$'s are the experimental values of masses and decay constants. With this definition, we have RMSPE $= 14.8\%$ for bottomonium.

Now, in order to analyze the case of a rotating plasma, with homogeneous angular velocity, we consider an AdS$_5$ space with cylindrical symmetry by writing the metric as

$$\mathrm{d}s^2 = \frac{R^2}{z^2}\left(-f(z)\mathrm{d}t^2 + \ell^2\mathrm{d}\varphi^2 + (\mathrm{d}x^1)^2 + (\mathrm{d}x^2)^2 + \frac{1}{f(z)}\mathrm{d}z^2\right), \tag{8}$$

where R is again the AdS radius and ℓ is the hypercylinder radius.

As in Refs. [22,23,28], we introduce rotation via the Lorentz-like coordinate transformation

$$\begin{aligned} t &\to \gamma(t + \Omega\ell^2\varphi), \\ \varphi &\to \gamma(\Omega t + \varphi), \end{aligned} \tag{9}$$

with

$$\gamma = \frac{1}{\sqrt{1-\Omega^2\ell^2}}, \tag{10}$$

where Ω is the angular velocity of the rotation. With this transformation, the metric (8) becomes

$$\begin{aligned} ds^2 = \frac{R^2}{z^2}\Big[&-\gamma^2(f(z)-\Omega^2\ell^2)dt^2 + 2\gamma^2(1-f(z))\Omega\ell^2 dt d\varphi \\ &+ \gamma^2(1-\Omega^2\ell^2 f(z))\ell^2 d\varphi^2 + (dx^1)^2 \\ &+ (dx^2)^2 + \frac{1}{f(z)}dz^2\Big], \end{aligned} \tag{11}$$

The temperature of the rotating AdS black hole is [22,23,28]

$$T = \frac{1}{\pi z_h}\sqrt{1-\Omega^2\ell^2}. \tag{12}$$

Note that we recover (8) by doing $\Omega \to 0$ in (11).

We assume that the rotating black hole metric of Eq. (11) is dual to a cylindrical slice of the rotating plasma. This interpretation can be justified by analyzing the angular momentum J. For the metric (11), J can be calculated [28] with the result

$$J = -\frac{\partial\Phi}{\partial\Omega} = \frac{2L^3}{\kappa^2}\frac{\Omega}{z_h^4(1-\Omega^2\ell^2)}, \tag{13}$$

while for the metric (8) one has $J = 0$. Thus, the coordinate transformation is adding angular momentum to the system and therefore representing a plasma in rotation.

III. EQUATIONS OF MOTION

By extremizing the action (4), we find the equations of motion

$$\partial_n(\sqrt{-g}e^{-\phi}F^{mn}) = 0. \tag{14}$$

We now choose a Fourier component of the field and, for simplicity, consider zero momentum (meson at rest), $V_m(t,\boldsymbol{x},z) = v_m(\omega,z)e^{-i\omega t}$. We also choose the gauge $V_z = 0$. The equations of motion (14) become

$$\frac{1-\Omega^2\ell^2 f}{1-\Omega^2\ell^2}\frac{\omega^2}{f^2}v_i + \left(\frac{f'}{f}-\frac{1}{z}-\phi'\right)v_i' + v_i'' = 0 \quad (i=1,2), \tag{15}$$

$$\begin{aligned} &-\left[\frac{1}{1-\Omega^2\ell^2 f^{-1}}\frac{f'}{f} + \frac{1-f}{f-\Omega^2\ell^2}\left(\frac{1}{z}+\phi'\right)\right]\Omega\ell^2 v_t' \\ &+\frac{1-f}{f-\Omega^2\ell^2}\Omega\ell^2 v_t'' + \frac{1-\Omega^2\ell^2}{1-\Omega^2\ell^2 f^{-1}}\frac{\omega^2}{f^2}v_\varphi \\ &+\left[\frac{1}{1-\Omega^2\ell^2 f^{-1}}\frac{f'}{f}-\frac{1}{z}-\phi'\right]v_\varphi' + v_\varphi'' = 0, \end{aligned} \tag{16}$$

$$\begin{aligned} &\left[\frac{1}{f^{-1}-\Omega^2\ell^2}\frac{f'}{f} + \frac{1-f}{1-\Omega^2\ell^2 f}\left(\frac{1}{z}+\phi'\right)\right]\Omega v_\varphi' \\ &-\frac{1-f}{1-\Omega^2\ell^2 f}\Omega v_\varphi'' - \left[\frac{1}{(\Omega^2\ell^2 f)^{-1}-1}\frac{f'}{f}+\frac{1}{z}+\phi'\right]v_t' + v_t'' = 0 \end{aligned} \tag{17}$$

and

$$v_t' - \frac{1-f}{1-\Omega^2\ell^2 f}\Omega v_\varphi' = 0, \tag{18}$$

where the prime stands for the derivative with respect to z, $f^{-1} = 1/f$, and, for simplicity, we omit the dependence on z of f and ϕ and the dependence on (ω, z) of the fields v_μ. These equations are not all independent, if we substitute (18) into (17) we obtain an identity, and substituting the same equation into (16), we obtain an equation for v_φ only. With this, the system of equations of motion simplifies to

$$\frac{1-\Omega^2\ell^2 f}{1-\Omega^2\ell^2}\frac{\omega^2}{f^2}v_i + \left(\frac{f'}{f}-\frac{1}{z}-\phi'\right)v_i' + v_i'' = 0 \quad (i=1,2), \tag{19}$$

$$\frac{1-\Omega^2\ell^2 f}{1-\Omega^2\ell^2}\frac{\omega^2}{f^2}v_\varphi + \left(\frac{1}{1-\Omega^2\ell^2 f}\frac{f'}{f}-\frac{1}{z}-\phi'\right)v_\varphi' + v_\varphi'' = 0, \tag{20}$$

$$v_t' - \frac{1-f}{1-\Omega^2\ell^2 f}\Omega v_\varphi' = 0. \tag{21}$$

Note that when $\Omega\ell = 0$, Eqs. (19) and (20) are the same and the two states are degenerate. Rotation breaks this degeneracy.

From this point on, we will divide our analysis in two cases, according to three possible polarizations. The first case is for polarizations in directions x^1 and x^2, for which $(v_m) = (0,v,0,0,0)$ or $(v_m) = (0,0,v,0,0)$. The second case is for the polarization in direction φ, for which $(v_m) = (0,0,0,v,0)$.

IV. SOLVING THE EQUATIONS OF MOTION

A. Near the horizon behavior of the solution

By approximating the function f as the first term of its power series at $z = z_h$, we write

$$f(z) \simeq f'(z_h)(z-z_h) \quad (\text{for } z \simeq z_h) \tag{22}$$

and we see that, in this region, Eqs. (19) and (20) both take the form

$$\frac{\gamma^2\omega^2}{f'(z_h)^2(z-z_h)^2}v_{\mathrm{hor}}(z)+\frac{1}{z-z_h}v'_{\mathrm{hor}}(z)+v''_{\mathrm{hor}}(z)=0, \quad (23)$$

which, in terms of the temperature, can be written as

$$\frac{\omega^2}{(4\pi T)^2}v_{\mathrm{hor}}(z)+(z-z_h)v'_{\mathrm{hor}}(z)+(z-z_h)^2v''_{\mathrm{hor}}(z)=0. \quad (24)$$

The two solutions of this equation are

$$\left(1-\frac{z}{z_h}\right)^{-\mathrm{i}\omega/4\pi T} \quad \text{and} \quad \left(1-\frac{z}{z_h}\right)^{+\mathrm{i}\omega/4\pi T}. \quad (25)$$

The solution with the minus sign in the exponent corresponds to an infalling wave at the horizon, while the other, with positive sign, corresponds to an outgoing wave. This becomes clear if one change to the Regge-Wheeler tortoise coordinate, as explained in Refs. [35,36].

The black hole allows only infalling waves at the horizon. Therefore, the field that solves the complete equations of motion has to obey the condition

$$v(z)\simeq A\left(1-\frac{z}{z_h}\right)^{-\mathrm{i}\omega/4\pi T} \quad (\text{for } z\simeq z_h), \quad (26)$$

where A is a normalization constant. The norm of the field will have no importance for us, then we can set $A=1$.

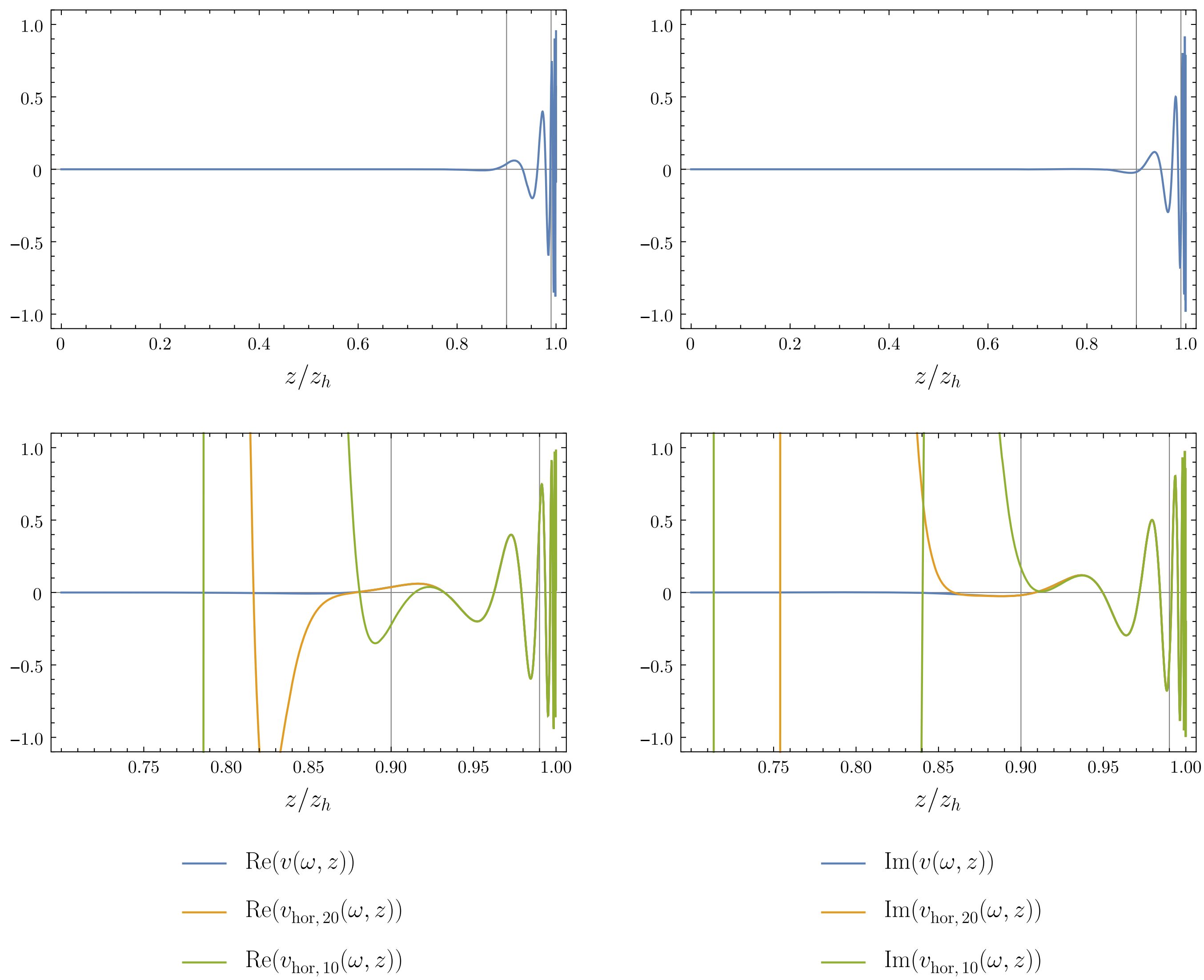

FIG. 1. Real (left) and Imaginary (right) parts of the field $v(\omega,z)$ (blue) and its approximations near the horizon $v_{\mathrm{hor},p}(\omega,z)$ with 20 (orange) and 10 (green) coefficients for the representative value of $\omega=10$ GeV for the nonrotating plasma at temperature $T=150$ MeV. In the first line we plot the field in all its domain. In the second line we zoom in the region from $z=0.7z_h$ to $z=z_h$. The vertical lines highlight the values $z=0.9z_h$ and $z=0.99z_h$.

In order to solve the complete equations of motion (19) and (20) numerically, we translate the infalling wave condition at the horizon in two boundary conditions to be imposed at a point $z = z_0$ close to the horizon,

$$v(z_0) = v_{\mathrm{hor},p}(z_0) \quad \text{and} \quad v'(z_0) = v'_{\mathrm{hor},p}(z_0), \tag{27}$$

with

$$v_{\mathrm{hor},p}(z) = \left(1 - \frac{z}{z_h}\right)^{-\mathrm{i}\omega/4\pi T} \sum_{n=0}^{p} a_n \left(1 - \frac{z}{z_h}\right)^n. \tag{28}$$

The function $v_{\mathrm{hor},p}(z)$ is just the infalling wave expression (26) (with A set to 1) times a polynomial correction of order p introduced for purposes of the numerical calculations. The coefficient a_0 is, of course, 1 and the other coefficients a_n are determined by imposing the equation of motion (19) or (20) with $v = v_{\mathrm{hor},p}$ to be valid up to the order p. The coefficients a_n are, therefore, the same for polarization in directions x^1 and x^2 but are different from the ones for polarization in the direction φ. The point z_0 is a chosen value of z, close to z_h, where the approximation $v(z) \simeq v_{\mathrm{hor},p}(z)$ is valid. Using Eq. (26), the leading term of the field, for z close to z_h, can be written as

$$\cos\left[\frac{\omega}{4\pi T}\ln\left(1 - \frac{z}{z_h}\right)\right] - \mathrm{i}\sin\left[\frac{\omega}{4\pi T}\ln\left(1 - \frac{z}{z_h}\right)\right]. \tag{29}$$

In the region of values of z close to the horizon, very small changes in z produce significant changes in $v(z)$, a problem for the numerical calculation. For this reason, the point z_0 cannot be chosen too close to z_h. This is the reason why we introduce the polynomial perturbation from (28) in the infalling condition. In this work, the value $z_0 = 0.9 z_h$ with 20 coefficients a_n was sufficient.

Figure 1 shows the solution of the equation of motion for the nonrotating plasma at a specific temperature and for some representative value of ω as well as two approximations for this solution near the horizon. From this figure, one can see that if we had chosen $z_0 = 0.99 z_h$, for example, instead of $z_0 = 0.9 z_h$, we would be in the unstable region and any small numerical error would be significantly propagated. Also, if we had used 10 coefficients, for example, instead of 20, we would not have a good approximation for the field at $z_0 = 0.9 z_h$. For more discussion on this method, see, for example, [37].

This method produces a numerical solution of Eqs. (19) or (20) with the infalling wave condition at z_h for any value of ω. We will use these solutions to calculate spectral functions and quasinormal modes in the following sections.

V. SPECTRAL FUNCTIONS

Spectral functions are defined in terms of the retarded Green's functions as

$$\varrho_{\mu\nu}(\omega) = -2\mathrm{Im}G^R_{\mu\nu}(\omega). \tag{30}$$

They provide an important way of analyzing the dissociation of quarkonia in a thermal medium. At zero temperature, the spectral function of a quarkonium, considering just one particle states, is a set of delta peaks at the values of the holographic masses of Table I. At finite temperature, these peaks acquire a finite height and a nonzero width. As the temperature increases the height of each peak decreases and its width increases. This broadening effect of the peaks indicates dissociation in the medium. In this section we calculate the spectral function for bottomonium in a rotating plasma at three fixed temperatures in order to analyze the effect of the rotational speed in the dissociation process.

A. Retarded Green's function

In the four-dimensional vector gauge theory we define a retarded Green's functions of the currents J_ν, that represent the heavy vector mesons, as

$$G^R_{\mu\nu} = -\mathrm{i}\int \mathrm{d}^4x e^{-\mathrm{i}p\cdot x}\Theta(t)\langle[J_\mu(x), J_\nu(0)]\rangle. \tag{31}$$

The Son-Starinets prescription [38] provide a way of extracting the retarded Green's function from the on shell action of the dual vector fields in AdS space

$$\begin{aligned} I_{\text{on shell}} &= -\frac{1}{4g_5^2}\int \mathrm{d}^4x \int_0^{z_h} \mathrm{d}z\sqrt{-g}\, e^{-\phi(z)} F_{mn}F^{mn} \\ &= -\frac{1}{2g_5^2}\int \mathrm{d}^4x \int_0^{z_h} \mathrm{d}z\partial_m(\sqrt{-g}\, e^{-\phi(z)} V_n F^{mn}), \end{aligned} \tag{32}$$

where we have used the equations of motion, (14), to go from the first line to the second.

In the gauge $V_z = 0$, we have $V_n F^{mn} = V_\nu F^{m\nu}$ and, therefore,

$$\begin{aligned} I_{\text{on shell}} = -\frac{1}{2g_5^2}\Bigg[&\int \mathrm{d}x^1\mathrm{d}x^2\mathrm{d}\varphi\mathrm{d}z\sqrt{-g}\, e^{-\phi(z)}V_\nu F^{t\nu}\Big|_{t=-\infty}^{t=+\infty} \\ &+ \int \mathrm{d}t\mathrm{d}x^2\mathrm{d}\varphi\mathrm{d}z\sqrt{-g}\, e^{-\phi(z)}V_\nu F^{1\nu}\Big|_{x^1=-\infty}^{x^1=+\infty} \\ &+ \int \mathrm{d}t\mathrm{d}x^1\mathrm{d}\varphi\mathrm{d}z\sqrt{-g}\, e^{-\phi(z)}V_\nu F^{2\nu}\Big|_{x^2=-\infty}^{x^2=+\infty} \\ &+ \int \mathrm{d}t\mathrm{d}x^1\mathrm{d}x^2\mathrm{d}z\sqrt{-g}\, e^{-\phi(z)}V_\nu F^{\varphi\nu}\Big|_{\varphi=0}^{\varphi=2\pi} \\ &+ \int \mathrm{d}^4x\sqrt{-g}\, e^{-\phi(z)}V_\nu F^{z\nu}\Big|_{z=0}^{z=z_h}\Bigg]. \end{aligned} \tag{33}$$

Since any physical field has to go to zero as t, x^1 or x^2 goes to $\pm\infty$, the first three terms vanish. The point with $\varphi = 0$ is equivalent to the point $\varphi = 2\pi$, therefore, the fourth term vanishes too. This leaves us just with the surface term

$$I_{\text{on shell}} = -\frac{1}{2g_5^2}\int d^4x\sqrt{-g}\, e^{-\phi(z)}V_\nu F^{z\nu}\Big|_{z=0}^{z=z_h}. \quad (34)$$

In momentum space and considering the meson at rest, we find

$$I_{\text{on shell}} = -\frac{1}{2g_5^2}\int d\omega\sqrt{-g}e^{-\phi(z)}\, g^{zz}\, g^{\mu\nu}\, v_\mu(-\omega,z)v'_\nu(\omega,z)\Big|_{z=0}^{z=z_h}. \quad (35)$$

Using the equation of motion (18) to substitute v'_t in terms of v'_φ, one eliminates v_t ending up with

$$I_{\text{on shell}} = -\frac{1}{2g_5^2}\int d\omega\sqrt{-g}e^{-\phi(z)}\, g^{zz} \times\left\{\sum_{j=1,2} g^{jj}v_j(-\omega,z)v'_j(\omega,z) + \left[\frac{(g^{t\varphi})^2}{-g^{tt}}+g^{\varphi\varphi}\right]v_\varphi(-\omega,z)v'_\varphi(\omega,z)\right\}\Big|_{z=0}^{z=z_h}. \quad (36)$$

Now we separate the value of the field at the boundary $z = 0$ by defining the bulk to boundary propagator $\mathcal{E}_\mu(\omega, z)$ such that

$$v_\mu(\omega,z) = \mathcal{E}_\mu(\omega,z)v_\mu^0(\omega) \quad (\text{no summation},\ \mu = 1,2,\varphi), \quad (37)$$

with $v_\mu^0(\omega) = v_\mu(\omega, 0)$. This implies the bulk to boundary condition $\mathcal{E}_\mu(\omega, 0) = 1$. Using the definition (37) in Eq. (36), the on shell action becomes

$$I_{\text{on shell}} = -\frac{1}{2g_5^2}\int d\omega\sqrt{-g}\, e^{-\phi(z)}\, g^{zz} \times\left\{\sum_{j=1,2} g^{jj}\mathcal{E}_j(-\omega,z)v_j^0(-\omega)\mathcal{E}'_j(\omega,z)v_j^0(\omega) + \left[\frac{(g^{t\varphi})^2}{-g^{tt}}+g^{\varphi\varphi}\right]\mathcal{E}_\varphi(-\omega,z)v_\varphi^0(-\omega) \times\mathcal{E}'_\varphi(\omega,z)v_\varphi^0(\omega)\right\}\Big|_{z=0}^{z=z_h}. \quad (38)$$

Then, applying the Son-Starinets prescription, we determine the retarded Green's functions

$$G_{jj}^R(\omega) = -\frac{\ell R}{g_5^2}e^{-\phi(0)}\lim_{z\to 0}\frac{1}{z}\mathcal{E}'_j(\omega,z) \quad (\text{no summation},\ j = 1,2) \quad (39)$$

and

$$G_{\varphi\varphi}^R(\omega) = -\frac{R}{\ell g_5^2}e^{-\phi(0)}\lim_{z\to 0}\frac{1}{z}\mathcal{E}'_\varphi(\omega,z). \quad (40)$$

The other $G_{\mu\nu}^R$ vanish.

In vacuum ($T = 0$), the Green's function is just

$$\Pi(p^2) = \sum_{n=1}^{\infty}\frac{f_n^2}{-p^2 - m_n^2 + i\varepsilon}, \quad (41)$$

where m_n and f_n are the mass and decay constant of the radial states of excitation level n of bottomonium. The imaginary part of this Green's function and, hence, the spectral function at zero temperature is proportional to

$$\sum_{n=1}^{\infty} f_n\delta(p^2 + m_n^2), \quad (42)$$

a set of delta peaks, each one located at the mass m_n of a state.

When the meson is inside a thermal medium, at a nonzero temperature, the change in the spectral function is a broadening of the peaks. These peaks acquire a finite height and a nonzero width. This broadening effect rises with the temperature and with the excitation level n and is interpreted as dissociation in the thermal medium. Variations of the spectral function of quarkonia in a thermal medium without rotation can be found on [8–11]. The same holographic model considered here was used in these references.

B. Numerical results of spectral functions

Figure 2 shows how bottomonium's spectral function changes with the rotation speed $\Omega\ell$ at temperature $T = 150$ MeV. Figures 3 and 4 do the same for temperatures fixed at $T = 200$ MeV and $T = 250$ MeV, respectively. In these charts we multiplied the spectral functions by the inverse of the constants that appear in Eqs. (39) and (40) in order to represent functions with the same dimension, that can be compared. From these figures one can see that rotation increases the dissociation effect and also that fields with polarization v_1 and v_2 dissociate slightly faster than the ones with polarization v_φ.

VI. QUASINORMAL MODES

In vacuum, the equations of motion simplify to

$$\omega^2 v + \left(-\frac{1}{z} - \phi'\right)v' + v'' = 0. \quad (43)$$

In this case, there is no black hole and, therefore, no infalling wave condition. We determine the normal modes by solving these equations with the exigence of the field to satisfy the normalization condition

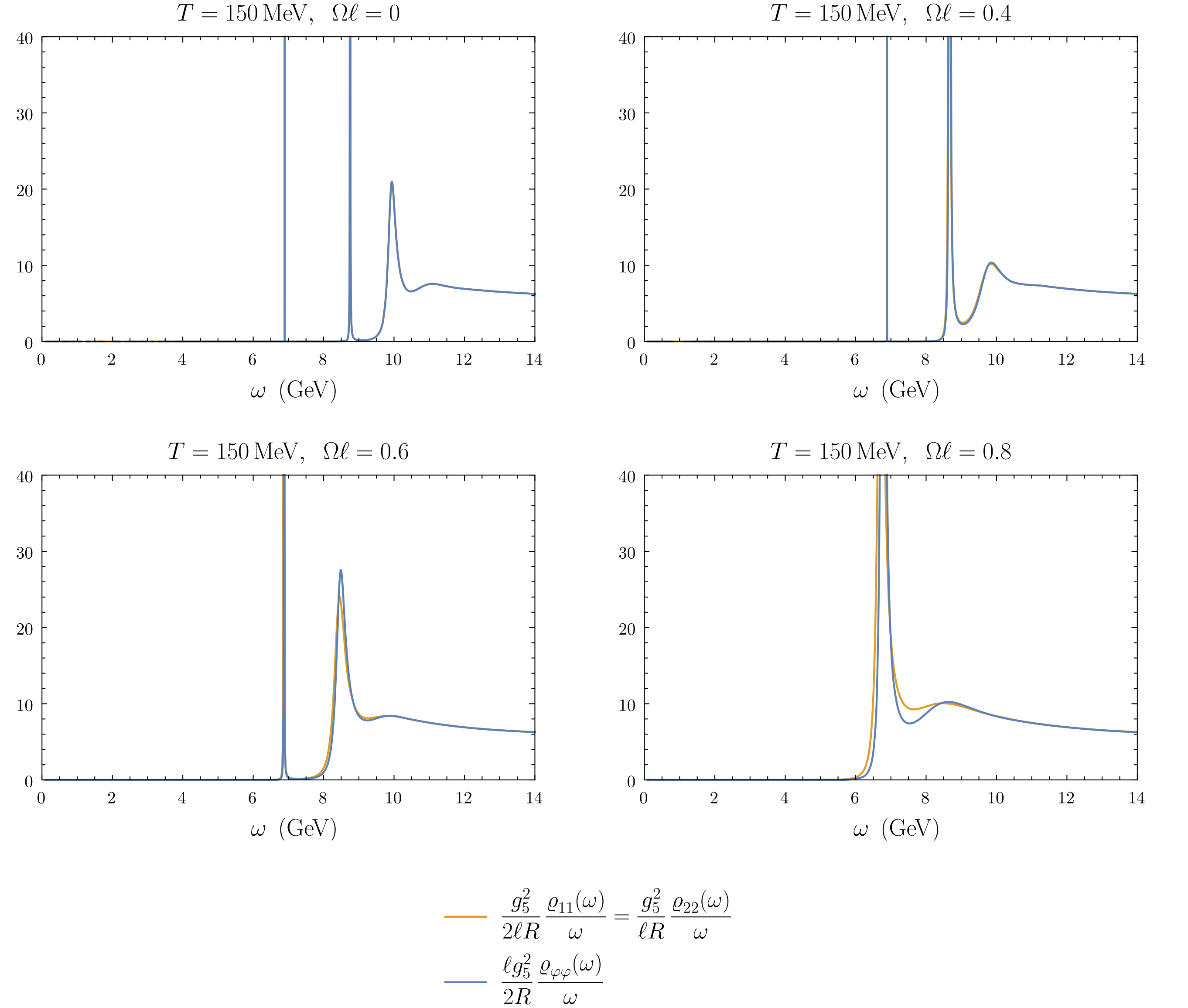

FIG. 2. Spectral functions $\varrho_{11}(\omega) = \varrho_{22}(\omega)$ and $\varrho_{\varphi\varphi}(\omega)$ for different values of rotation speed $\Omega\ell$ and temperature fixed at $T = 150$ MeV.

$$\int_0^\infty \frac{R}{z} e^{-\phi(z)} |v(z)|^2 dz = 1. \tag{44}$$

It is possible to translate this normalization condition into the Dirichlet condition

$$v(\omega, z = 0) = 0. \tag{45}$$

This equation is solvable only for a discrete set of real values ω_n. These values are the masses of the quarkonium states in vacuum. They are shown in the third column of Table I.

At finite temperature, instead of normal modes, we have the quasinormal modes. They are the solutions of the equations of motion (19) and (20), that satisfy:

(1) the infalling wave condition at the horizon; and
(2) the Dirichlet condition (45).

The values ω_n that satisfy both of this conditions are called quasinormal frequencies, the fields $v_\mu(\omega_n, z)$ are called quasinormal modes and represent the meson quasistates.

As the value at $T = 0$ of the normal frequency ω_n is interpreted as the mass of the particle in its state n, the real part of the quasinormal frequency $\mathrm{Re}(\omega_n)$, at finite temperature, is interpreted as the thermal mass of the quasiparticle. The imaginary part $\mathrm{Im}(\omega_n)$ is related to its degree of dissociation. The larger the absolute value of the imaginary part, the stronger the dissociation. It is interesting to note that the real and imaginary parts of a nth quasinormal mode are related to the position and width of the nth peak in the spectral function. Therefore, we can interpret a growth in

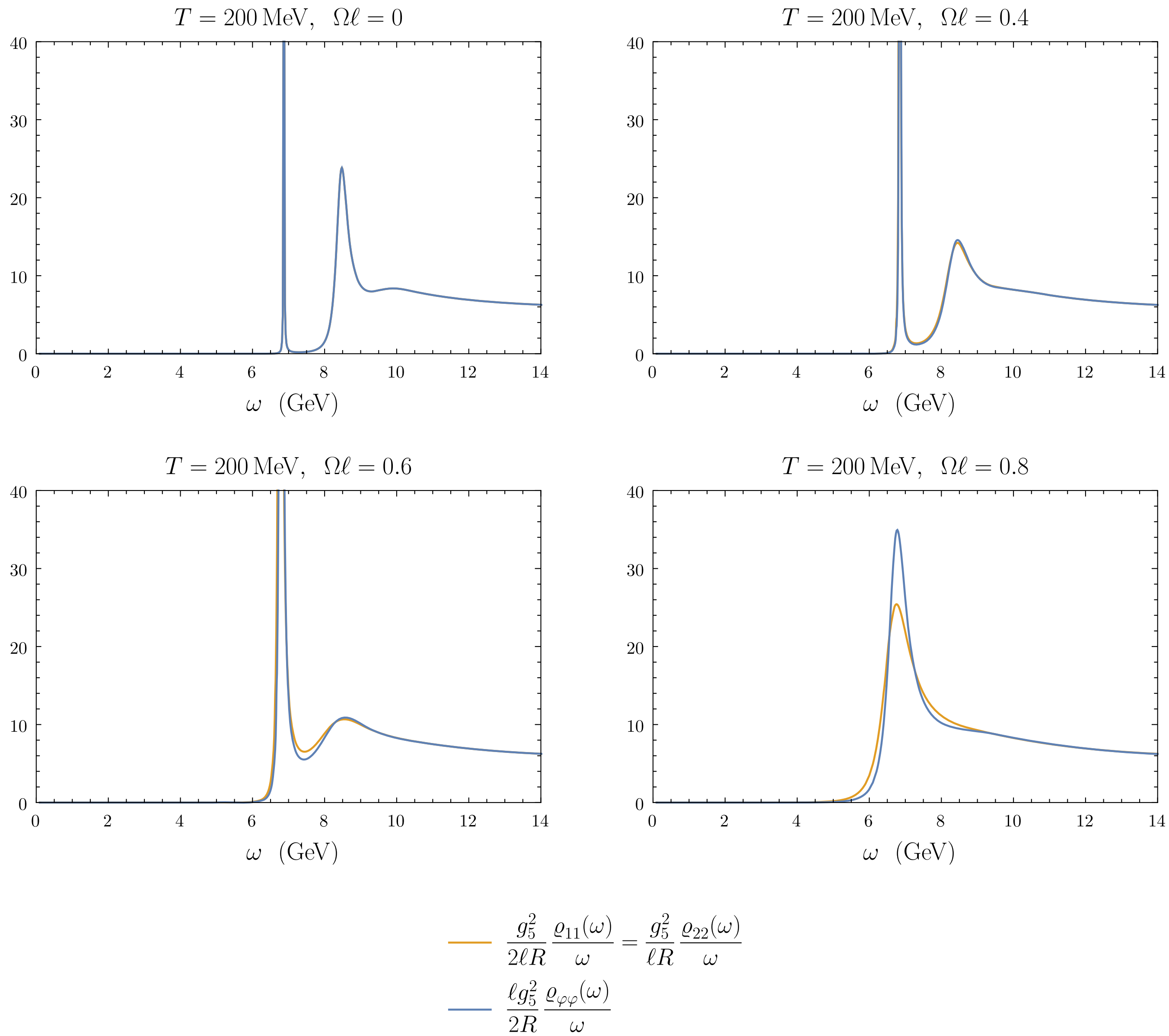

FIG. 3. Spectral functions $\varrho_{11}(\omega) = \varrho_{22}(\omega)$ and $\varrho_{\varphi\varphi}(\omega)$ for different values of rotation speed $\Omega\ell$ and temperature fixed at $T = 200$ MeV.

the imaginary part of the quasinormal frequency as an increase in the dissociation effect. Indeed, at $T = 0$ the width of the spectral function peaks is zero, as is the imaginary part of the frequency ω_n. Also, the limit for $T \to 0$ of $\mathrm{Re}(\omega_n)$ is the mass m_n. This discussion for the nonrotating plasma with temperature only is already present in the literature. One can find an application of the tangent model for this case on Refs. [8–11].

The results of quasinormal frequencies for polarizations x^j and φ as function of the rotation speed $\Omega\ell$ and for temperature fixed at $T = 200$ MeV are shown in Fig. 5. From this figure, one sees that the dissociation degree, measured by $-\mathrm{Im}(\omega)$, rises with the rotation speed $\Omega\ell$.

VII. CONCLUSIONS

We analyzed in this work how the rotation of a quark gluon plasma affects the thermal dissociation of heavy vector mesons that are inside the medium. The motivation for such a study is the fact that noncentral heavy ion collisions lead to the formation of a QGP with high angular momentum. So, a description of quarkonium inside the plasma should take rotation into account. We considered, as an initial study, the case of a cylindrical shell of plasma in rotation about the symmetry axis. The real case of the QGP should involve a volume rather than a cylindrical hypersurface and also possible interaction between different layers of the plasma, that would have different rotational

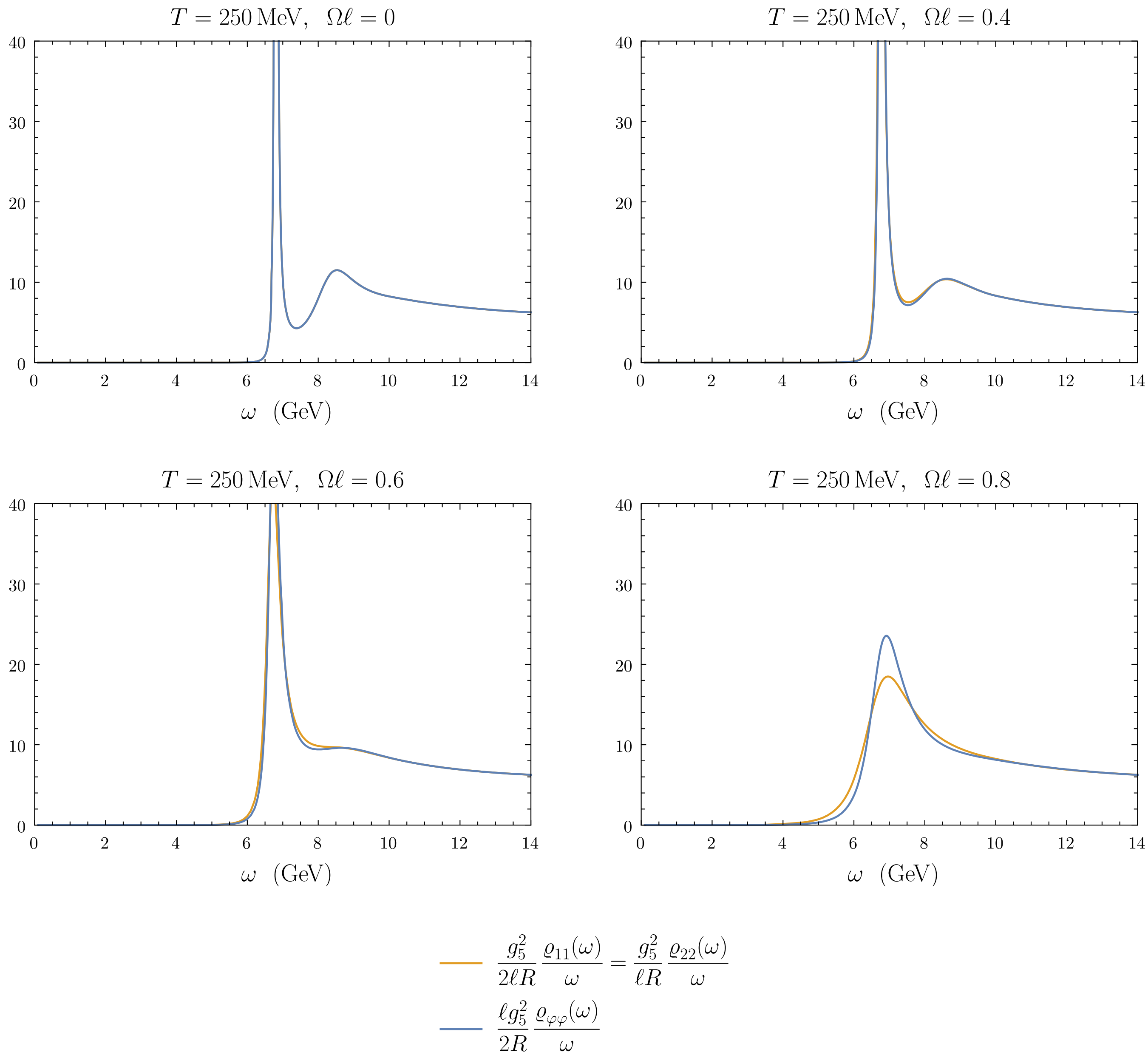

FIG. 4. Spectral functions $\varrho_{11}(\omega) = \varrho_{22}(\omega)$ and $\varrho_{\varphi\varphi}(\omega)$ for different values of rotation speed $\Omega\ell$ and temperature fixed at $T = 250$ MeV.

speeds. However this simple case considered here already provides important nontrivial information. It is clear from the results obtained here that rotation enhances the dissociation process for heavy vector mesons inside a plasma. It was also found that this effect caused by rotation is more intense for heavy vector mesons that have polarization perpendicular to the rotational velocity of the meson.

In the holographic approach used here, the bottomonium quasistates are represented by classical vector fields. In this framework the polarization corresponds just to the direction of the field, that is not affected by the rotation of the medium. It is important to mention that there is an important aspect of the actual physical problem of heavy vector mesons inside a rotating plasma that does not show up in this holographic approach. Namely, the coupling of the spin of the mesons to the angular momentum of the medium. Such a coupling affects the dissociation, in a way that depends on the relation between the direction of rotation of the medium and the direction of the spin. Also, in a quantum process, like the heavy ion collision, the states that are created can not be described as pure spin states but rather by density matrices, since they represent mixed states. It would be an interesting issue to be explored in future work to look for a holographic description of the interaction (coupling)

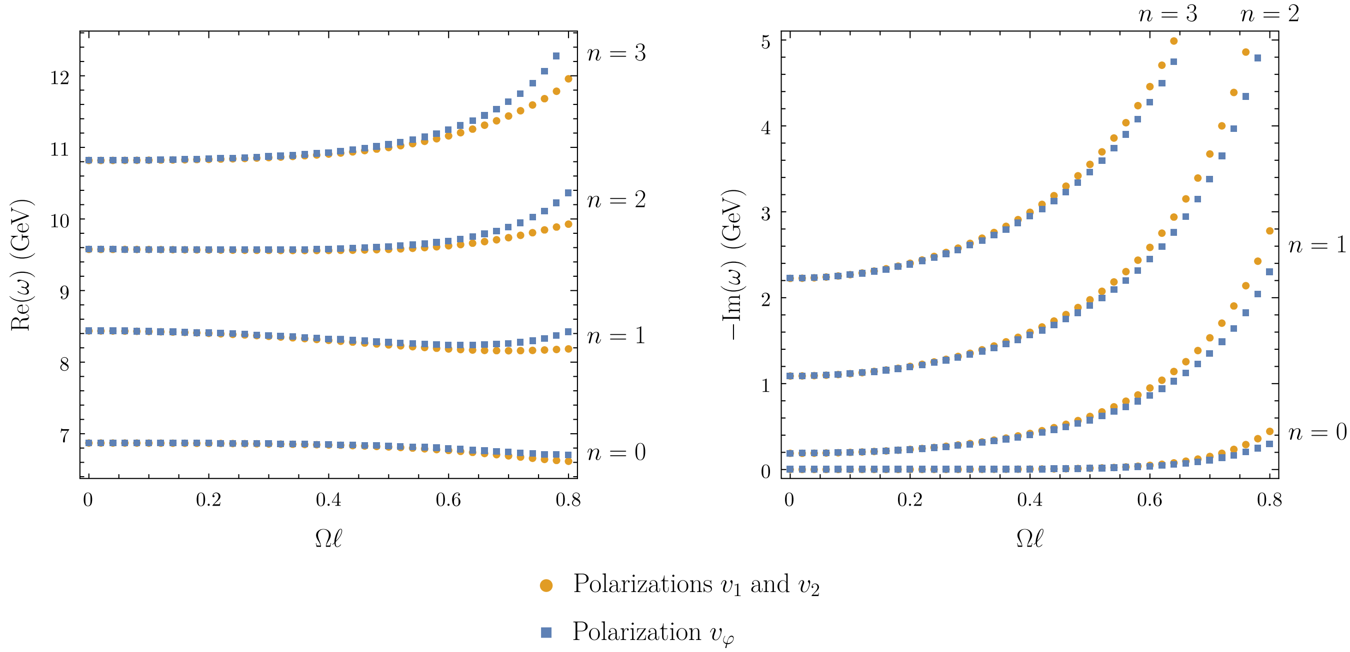

FIG. 5. Quasinormal frequencies of the different excitation levels as functions of the rotation speed $\Omega\ell$ and temperature fixed at $T = 200$ MeV.

between the meson spin and the QGP angular momentum and the effect that such interaction has on spin alignment. For interesting discussions about this issue, see [39,40]. In these references the mesons are not described by dual supergravity classical fields, as happens in the holographic case presented here, but rather as particles with dynamics described by some Hamiltonian that includes the coupling between the angular momentum of the plasma and the spin of the meson. It would be very nice to find a way to represent this coupling in the holographic framework since there are interesting recent works that propose forms of measuring the density matrix of quarkonium [39–42] and also a recent measurement of quarkonium polarization in heavy ion collisions [43].

Finally, it is interesting to discuss the possibility of describing mixed states using the holographic approach. Or, in other words, how could one define a density matrix in the present framework. We are describing vector mesons, that are spin one particles, in terms of vector fields. In order to build up a density matrix one needs to define a convenient basis of spin states. The natural choice is the set of three states with $j = 1$ and $m = -1, 0, +1$, corresponding, as usual, to the eigenvalue of total spin and of the spin projection in some direction, taken in general as x_3.

In the case of vectors in Cartesian coordinates, the transformation from the Cartesian components V_1, V_2, V_3 to the eigenstates of j and m is simply a transformation to a spherical tensors of rank 1. Writing the eigenstates of j and m as $V_m^{(j)}$ on can write

$$V_{+1}^{(1)} = -\frac{1}{\sqrt{2}}(V_1 + iV_2); \qquad V_0^{(1)} = V_3;$$
$$V_{-1}^{(1)} = \frac{1}{\sqrt{2}}(V_1 - iV_2). \tag{46}$$

These relations imply that one can obtain, for example, the state $V_{+1}^{(1)}$ by simply choosing a solution for the Cartesian fields satisfying $V_2 = -iV_1$ and $V_3 = 0$. The other states are obtained in a similar way. Once the basis is defined, the density matrix elements are defined as $\langle V_m^{(1)}|\rho|V_{m'}^{(1)}\rangle$, where ρ is the usual density operator that contains the information about the state.

In the present case there is subtlety. We considered a particular situation of a plasma where all the points rotate with the same speed; not only the same angular speed but also the same radius. In order to achieve this we deformed the original space, compactifying one coordinate, as can be seen comparing Eq. (1) with Eq. (8). So, our geometry on the boundary, that is the plasma geometry, is that of a hypercylinder with two coordinates perpendicular to the rotation circle, spanned by coordinate φ. We chose this approach since the coordinate transformation involves the speed of rotation, and thus the dual black hole depends on it. So, it is reasonable to start such a holographic calculation of spectral functions and quasinormal modes with a simplified model involving just one black hole geometry. In the recent work [44] the case of a volumetric rotating plasma was described by superimposing different cylindrical shells, each one with a dual black hole description.

Using such a volumetric geometry, where the radius ρ is not constant but a coordinate and suppressing one of the coordinates x_1 or x_2, with the other becoming the rotational axis, one would deal with standard vector fields in cylindrical coordinates. These field could than be related to the spherical tensor of rank 1 that form the basis that is necessary in order to build up a density matrix. It would be interesting to investigate this situation in the future.

ACKNOWLEDGMENTS

N. R. F. B. is partially supported by CNPq—Conselho Nacional de Desenvolvimento Científico e Tecnológico Grant No. 307641/2015-5 and by FAPERJ—Fundação Carlos Chagas Filho de Amparo à Pesquisa do Estado do Rio de Janeiro. The authors received also support from Coordenação de Aperfeiçoamento de Pessoal de Nível Superior—Brasil (CAPES), Finance Code 001.

[1] S. A. Bass, M. Gyulassy, H. Stoecker, and W. Greiner, Signatures of quark gluon plasma formation in high-energy heavy ion collisions: A critical review, J. Phys. G **25**, R1 (1999).

[2] S. Scherer *et al.*, Critical review of quark gluon plasma signatures, Prog. Part. Nucl. Phys. **42**, 279 (1999).

[3] E. Shuryak, Physics of strongly coupled quark-gluon plasma, Prog. Part. Nucl. Phys. **62**, 48 (2009).

[4] J. Casalderrey-Solana, H. Liu, D. Mateos, K. Rajagopal, and U. A. Wiedemann, *Gauge/String Duality, Hot QCD and Heavy Ion Collisions* (Cambridge University Press, Cambridge, England, 2014).

[5] N. R. F. Braga, M. A. Martin Contreras, and S. Diles, Decay constants in soft wall AdS/QCD revisited, Phys. Lett. B **763**, 203 (2016).

[6] N. R. F. Braga, M. A. Martin Contreras, and S. Diles, Holographic picture of heavy vector meson melting, Eur. Phys. J. C **76**, 598 (2016).

[7] N. R. F. Braga and L. F. Ferreira, Bottomonium dissociation in a finite density plasma, Phys. Lett. B **773**, 313 (2017).

[8] N. R. F. Braga, L. F. Ferreira, and A. Vega, Holographic model for charmonium dissociation, Phys. Lett. B **774**, 476 (2017).

[9] N. R. F. Braga and L. F. Ferreira, Heavy meson dissociation in a plasma with magnetic fields, Phys. Lett. B **783**, 186 (2018).

[10] N. R. F. Braga and L. F. Ferreira, Quasinormal modes and dispersion relations for quarkonium in a plasma, J. High Energy Phys. 01 (2019) 082.

[11] N. R. F. Braga and L. F. Ferreira, Quasinormal modes for quarkonium in a plasma with magnetic fields, Phys. Lett. B **795**, 462 (2019).

[12] M. A. Martin Contreras, S. Diles, and A. Vega, Heavy quarkonia spectroscopy at zero and finite temperature in bottom-up AdS/QCD, Phys. Rev. D **103**, 086008 (2021).

[13] R. Zöllner and B. Kämpfer, Holographic bottomonium formation in a cooling strong-interaction medium at finite baryon density, Phys. Rev. D **104**, 106005 (2021).

[14] L. A. H. Mamani, D. Hou, and N. R. F. Braga, Melting of heavy vector mesons and quasinormal modes in a finite density plasma from holography, Phys. Rev. D **105**, 126020 (2022).

[15] A. S. Miranda, J. Morgan, A. Kandus, and V. T. Zanchin, Separable wave equations for gravitoelectromagnetic perturbations of rotating charged black strings, Classical Quantum Gravity **32**, 235002 (2015).

[16] Y. Jiang and J. Liao, Pairing phase transitions of matter under rotation, Phys. Rev. Lett. **117**, 192302 (2016).

[17] B. McInnes, A rotation/magnetism analogy for the quark–gluon plasma, Nucl. Phys. **B911**, 173 (2016).

[18] L. A. H. Mamani, J. Morgan, A. S. Miranda, and V. T. Zanchin, From quasinormal modes of rotating black strings to hydrodynamics of a moving CFT plasma, Phys. Rev. D **98**, 026006 (2018).

[19] X. Wang, M. Wei, Z. Li, and M. Huang, Quark matter under rotation in the NJL model with vector interaction, Phys. Rev. D **99**, 016018 (2019).

[20] M. N. Chernodub, Inhomogeneous confining-deconfining phases in rotating plasmas, Phys. Rev. D **103**, 054027 (2021).

[21] I. Y. Aref'eva, A. A. Golubtsova, and E. Gourgoulhon, Holographic drag force in 5d Kerr-AdS black hole, J. High Energy Phys. 04 (2021) 169.

[22] X. Chen, L. Zhang, D. Li, D. Hou, and M. Huang, Gluodynamics and deconfinement phase transition under rotation from holography, J. High Energy Phys. 07 (2021) 132.

[23] J. Zhou, X. Chen, Y.-Q. Zhao, and J. Ping, Thermodynamics of heavy quarkonium in rotating matter from holography, Phys. Rev. D **102**, 126029 (2021).

[24] V. V. Braguta, A. Y. Kotov, D. D. Kuznedelev, and A. A. Roenko, Influence of relativistic rotation on the confinement-deconfinement transition in gluodynamics, Phys. Rev. D **103**, 094515 (2021).

[25] V. V. Braguta, A. Y. Kotov, D. D. Kuznedelev, and A. A. Roenko, Lattice study of the confinement/deconfinement transition in rotating gluodynamics, Proc. Sci. LATTICE2021 (**2022**) 125 [arXiv:2110.12302].

[26] A. A. Golubtsova, E. Gourgoulhon, and M. K. Usova, Heavy quarks in rotating plasma via holography, Nucl. Phys. **B979**, 115786 (2022).

[27] Y. Fujimoto, K. Fukushima, and Y. Hidaka, Deconfining phase boundary of rapidly rotating hot and dense matter and analysis of moment of inertia, Phys. Lett. B **816**, 136184 (2021).

[28] N. R. F. Braga, L. F. Faulhaber, and O. C. Junqueira, Confinement-deconfinement temperature for a rotating quark-gluon plasma, Phys. Rev. D **105**, 106003 (2022).

[29] Y. Chen, D. Li, and M. Huang, Inhomogeneous chiral condensation under rotation in the holographic QCD, Phys. Rev. D **106**, 106002 (2022).

[30] A. A. Golubtsova and N. S. Tsegel'nik, Nuclear the holographic model of $\mathcal{N} = 4$ SYM rotating quark-gluon plasma, Phys. Rev. D **107**, 106017 (2023).

[31] Y.-Q. Zhao, S. He, D. Hou, L. Li, and Z. Li, Phase diagram of holographic thermal dense QCD matter with rotation, J. High Energy Phys. 04 (2023) 115.

[32] M. N. Chernodub, V. A. Goy, and A. V. Molochkov, Inhomogeneity of rotating gluon plasma and Tolman-Ehrenfest law in imaginary time: Lattice results for fast imaginary rotation, Phys. Rev. D **107**, 114502 (2023).

[33] Y.-Q. Zhao and D. Hou, J/Ψ suppression in a rotating magnetized holographic QGP matter, arXiv:2306.04318.

[34] P. A. Zyla *et al.* (Particle Data Group), Review of particle physics, Prog. Theor. Exp. Phys. **2020**, 083C01 (2020).

[35] L. A. H. Mamani, A. S. Miranda, H. Boschi-Filho, and N. R. F. Braga, Vector meson quasinormal modes in a finite-temperature AdS/QCD model, J. High Energy Phys. 03 (2014) 058.

[36] A. S. Miranda, C. A. Ballon Bayona, H. Boschi-Filho, and N. R. F. Braga, Black-hole quasinormal modes and scalar glueballs in a finite-temperature AdS/QCD model, J. High Energy Phys. 11 (2009) 119.

[37] M. Kaminski, K. Landsteiner, F. Pena-Benitez, J. Erdmenger, C. Greubel, and P. Kerner, Quasinormal modes of massive charged flavor branes, J. High Energy Phys. 03 (2010) 117.

[38] D. T. Son and A. O. Starinets, Minkowski space correlators in AdS/CFT correspondence: Recipe and applications, J. High Energy Phys. 09 (2002) 042.

[39] K. J. Gonçalves and G. Torrieri, Spin alignment of vector mesons as a probe of spin hydrodynamics and freeze-out, Phys. Rev. C **105**, 034913 (2022).

[40] P. H. De Moura, K. J. Goncalves, and G. Torrieri, Quarkonium spin alignment in a vortical medium, Phys. Rev. D **108**, 034032 (2023).

[41] Z.-T. Liang and X.-N. Wang, Spin alignment of vector mesons in non-central A + A collisions, Phys. Lett. B **629**, 20 (2005).

[42] X.-L. Xia, H. Li, X.-G. Huang, and H. Zhong Huang, Local spin alignment of vector mesons in relativistic heavy-ion collisions, Phys. Lett. B **817**, 136325 (2021).

[43] S. Acharya *et al.* (ALICE Collaboration), First measurement of quarkonium polarization in nuclear collisions at the LHC, Phys. Lett. B **815**, 136146 (2021).

[44] N. R. F. Braga and O. C. Junqueira, Inhomogeneity of a rotating quark-gluon plasma from holography, arXiv:2306.08653.